Inorg. Chem. **2002**, *41*, 5336–5349

Structural and Photophysical Properties of Heterobimetallic 4f-Zn Iminophenolate Cryptates

Raquel Rodríguez-Cortiñas,[†] Fernando Avecilla,[†] Carlos Platas-Iglesias,[†] Daniel Imbert,[‡] Jean-Claude G. Bünzli,[‡] Andrés de Blas,*[,†] and Teresa Rodríguez-Blas*[,†]

Departamento de Química Fundamental, Universidade da Coruña, Campus da Zapateira, s/n 15071 A Coruña, Spain, and Institute of Molecular and Biological Chemistry, Swiss Federal Institute of Technology Lausanne, BCH 1402, CH-1015 Lausanne, Switzerland

Received March 12, 2002

Lanthanide complexes with the Schiff base axial macrobicyclic ligand L^1 react with Zn(II) nitrate in the presence of CaH_2 to yield Ln(III)–Zn(II) heterodinuclear cryptates with the formula $[Ln(NO_3)(L^1\text{-}3H)Zn](NO_3)\cdot x H_2O\cdot y MeOH$. The macrobicyclic receptor L^1 is an azacryptand $N[(CH_2)_2N{=}CH{-}R{-}CH{=}N{-}(CH_2)_2]_3N$ (R = 1,3-(2-OH-5-Me-C_6H_2)). The crystal structures of the Pr(III), Yb(III), and Lu(III) complexes, chemical formulas $[Ln(NO_3)(L^1\text{-}3H)Zn](NO_3)\cdot x$Solv (monoclinic, *C*2/*c*, $Z = 8$), as well as that of $[Zn_2(L^1\text{-}3H)](NO_3)\cdot H_2O$ (**15**) (triclinic, $P\bar{1}$, $Z = 2$), have been determined by X-ray crystallography. The ligand is helically wrapped around the two metal ions, leading to pseudo-C_3 symmetries around the metals. The Ln(III)–Zn(II) distances lie in the range 3.3252(13) to 3.2699(14) Å, while the Zn(II)–Zn(II) distance in **15** amounts to 3.1037(18) Å. The three five-membered chelate rings of the ligand backbone coordinating the Ln(III) ion adopt a $(\lambda\lambda\delta)_5$ (or $(\delta\delta\lambda)_5$) conformation while the three pseudochelate rings formed by the coordination of the ligand to the Zn(II) ion adopt a $(\lambda'\lambda'\lambda')_5$ (or $(\delta'\delta'\delta')_5$) conformation. Thus in the solid state the conformation of the three cations is $\Lambda(\delta\delta\lambda)_5(\delta'\delta'\delta')_5$ or its enantiomeric form $\Delta(\lambda\lambda\delta)_5(\lambda'\lambda'\lambda')_5$. In solution, the helicates present a time-averaged C_3 symmetry, as shown by ^{1}H NMR, and the conformation of the cations is described as $\Lambda(\delta\delta\delta)_5(\delta'\delta'\delta')_5$ (or $\Delta(\lambda\lambda\lambda)_5(\lambda'\lambda'\lambda')_5$). The photophysical properties of the cryptates depend on the nature of the Ln(III) ion, and $(L\text{-}3H)^{3-}$ is revealed to be a good sensitizer for Eu(III) and Tb(III) at low temperatures, but the emission at room temperature is limited by the low energy of the ligand $^3\pi\pi^*$ state. While Eu(III) is most effectively sensitized by the ligand triplet state, the Tb(III) ($^5D_4$) sensitization occurs via the singlet state. The quantum yield of the metal-centered luminescence in the Eu–Zn cryptate amounts to 1.05% upon ligand excitation. The low energy of the ligand $^3\pi\pi^*$ state allows efficient sensitization of the Nd(III) and Yb(III) cryptates, which emit in the near-infrared.

Introduction

Lanthanide coordination compounds[1] are the subject of intense research efforts due to their applications as contrast agents for NMR imaging,[2,3] as catalysts in RNA hydrolysis,[4] as active agents in cancer radiotherapy,[5] or as luminescent stains for protein labeling and sensitive homogeneous immunoassays.[6]

Among the receptors used to encapsulate the lanthanide(III) ions, macrocyclic platforms play an essential role,[7] especially for protecting the metal ion from external interactions and for generating a good antenna effect. Indeed, some lanthanide ions, such as Eu(III) and Tb(III), possess strongly emissive and long-lived excited states but do not exhibit intense absorption bands.[8] Therefore, considerable effort has been devoted to design lanthanide complexes where light is

* Address correspondence to these authors. E-mail: mayter@udc.es.
† Departamento de Química Fundamental, Universidade da Coruña.
‡ Swiss Federal Institute of Technology Lausanne.

(1) Bünzli, J.-C. G. *Rare Earths*; Saez-Puche, R., Caro, P., Eds.; Editorial Complutense: Madrid, Spain, 1998; p 223ff.
(2) Merbach, A. E.; Tóth, É. *The Chemistry of Contrast Agents in Medical Magnetic Resonance Imaging*; John Wiley & Sons: Chichester, UK, 2001.
(3) Peters, J. A.; Huskens, J.; Raber, D. J. *Prog. Magn. Reson. Spectrosc.* **1996**, *28*, 283.
(4) Roigk, A.; Hettich, R.; Schneider, H.-J. *Inorg. Chem.* **1998**, *37*, 751.
(5) DeNardo, G. L.; Mirik, G. R.; Kroger, L. A.; O'Donnel, R. T.; Meares, C. F.; DeNardo, S. L. *J. Nucl. Med.* **1996**, *37*, 451.
(6) Mathis, G. *Rare Earths*; Saez-Puche, R., Caro, P., Eds.; Editorial Complutense: Madrid, Spain, 1998.
(7) Alexander, V. *Chem. Rev.* **1995**, *95*, 273.

10.1021/ic025587s CCC: $22.00 © 2002 American Chemical Society
Published on Web 09/17/2002

Scheme 1

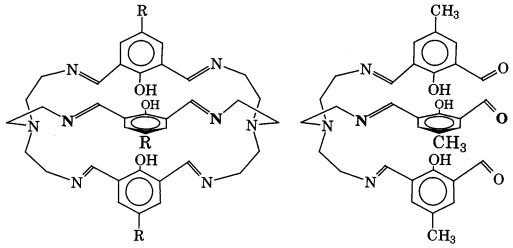

L¹: R = Me
L²: R = Cl
L³: R = *t*-Bu

L⁴

absorbed by the ligands and the corresponding electronic energy is then transferred onto the emitting metal ion. Analogous sensitization of Nd(III) and Yb(III), which emit in the near-infrared, has been the subject of some studies in recent years,[9] and opens interesting perspectives for tailoring new light-converting devices.

Monometallic cryptates with L^1 and L^3 (Scheme 1) have been obtained for Ln = Sc, Y, Gd, Eu, Tb, and Dy by transmetalation of the sodium derivatives.[10] In subsequent works, we have shown that the 1:1 cryptates $[LnL^1(NO_3)][Ln(NO_3)_5]\cdot xH_2O$ or $[LnL^1(NO_3)](NO_3)_2\cdot xH_2O$ (Ln = La − Lu, except Pm) can be obtained by direct template reaction[11] and we have reported their structure in both the solid state and aqueous solution,[12,13] as well as their photophysical properties and relaxivity.[14] The corresponding anionic cryptand $(L^1\text{-}3H)^{3-}$ is also able to accommodate two lanthanide(III) ions into the macrobicyclic cavity, yielding complexes with the formula $[Ln_2(L^1\text{-}3H)(NO_3)_2](NO_3)\cdot xH_2O\cdot y$EtOH (Ln = Gd to Lu).[15]

Increasing interest has been devoted to dinuclear complexes comprising simultaneously either 4f or 3d ions, which possess interesting luminescent and magnetic properties.[16,17] However, while macrocyclic[18] or podand[19−21] ligands have been widely used to prepare *4*f−3d complexes, we are aware of only two examples of cryptates of this type with the formulas $[DyCu(L^2\text{-}3H)(DMF)](ClO_4)_2\cdot MeCN$[22] and $[GdNi(L^2\text{-}3H)(DMF)](ClO_4)_2\cdot MeCN$,[23] the latter reported while our work was in progress. We have found that the iminophenolate cryptand L^1 is also able to simultaneously accommodate one lanthanide(III) and one zinc(II) ion, and in this paper we describe the first examples of 4f-Zn cryptates and report their photophysical properties, as well as a comparative structural study in the solid state and in solution.

Experimental Section

Materials. The mononuclear lanthanide cryptates $[LnL^1(NO_3)](NO_3)_2\cdot nH_2O$ were prepared as previously described.[12] Ligand L^4 was obtained in ethanol by a similar procedure to that reported previously by Schröder et al.[24] All other reagent-grade chemicals and solvents for synthesis were purchased from commercial sources and used without further purification. Acetonitrile-d_3 for NMR measurements (ACROS, 99% D) was used as received. Solvents for luminescence measurements were purchased from Fluka AG (Buchs, Switzerland) and used without further purification.

Preparation of the Complexes: $[CeZn(L^1\text{-}3H)(NO_3)](NO_3)\cdot 0.5H_2O$ (1). To a stirred solution of $[CeL^1(NO_3)](NO_3)_2\cdot 4H_2O$ (0.106 g; 0.1 mmol) in 20 mL of absolute methanol 50 μL of DMF and 0.0097 g (0.22 mmol) of CaH_2 were added. The resulting mixture was stirred for 48 h at room temperature and then filtered. The filtrate was added to a solution of $Zn(NO_3)_2\cdot 6H_2O$ (0.030 g; 0.1 mmol) in 5 mL of methanol, stirred, and heated to reflux for 7 h and then concentrated to 5−10 mL under vacuum. The complex was isolated as a red microcrystalline powder by slow diffusion of diethyl ether into this solution. Yield: 0.024 g (24%). Anal. Calcd for $C_{39}CeH_{45}N_{10}O_9Zn\cdot 0.5H_2O$: C, 46.3; H, 4.6; N, 13.8. Found: C, 46.4; H, 4.5; N, 13.5. Λ_m (Ω^{-1} cm^2 mol^{-1}): 179. MS-FAB (*m*/*z*): 939 [**1** − NO_3]. IR (KBr): 1636 cm^{-1}.

$[PrZn(L^1\text{-}3H)(NO_3)](NO_3)\cdot H_2O$ (2). The yellow complex was prepared as described for **1** by using $[PrL^1(NO_3)](NO_3)_2\cdot 2H_2O$ (0.104 g, 0.1 mmol). Yield: 0.011 g (11%). Anal. Calcd for $C_{39}H_{45}N_{10}O_9PrZn\cdot H_2O$: C, 45.8; H, 4.6; N, 13.7. Found: C, 46.1;

(8) Carnall, W. T. *Handbook on the Physics and Chemistry of Rare Earths*; Gschneidner, K. A., Jr., Eyring, L., Eds.; Elsevier: Amsterdam, The Netherlands, 1987; Vol. 3, p 171.

(9) (a) Shevchuk, S. V.; Alexeeva, E. A.; Rusakova, N. V.; Korovin, Y. V.; Bacherikov, V. A.; Gren, A. I. *Mendeleev Commun.* **1998**, *3*, 1998. (b) Hall, J.; Häner, R.; Aime, S.; Botta, M.; Faulkner, S.; Parker, D.; De Sousa, A. S. *New J. Chem.* **1998**, 627. (c) Beeby, A.; Dickins, R. S.; Faulkner, S.; Parker, D.; Gareth Williams, J. A. *Chem. Commun.* **1997**, 1401. (d) Horrocks, W. D., Jr.; Bolender, J. P.; Smith, W. D.; Supkowski, R. M. *J. Am. Chem. Soc.* **1997**, *119*, 5972. (e) Wolbers, M. P. O.; Van Veggel, F. C. J. M.; Peters, F. G. A.; Van Beelen, E. S. E.; Hofstraat, J. W.; Geurts, F. A. J.; Reinhoudt, D. N. *Chem. Eur. J.* **1998**, *4*, 772. (f) Yanagida, S.; Hasegawa, Y.; Murakoshi, K.; Wada, Y.; Nakashima, N.; Yamanaka, T. *Coord. Chem. Rev.* **1998**, *171*, 461.

(10) Drew, M. G. B.; Howarth, O. W.; Harding, C. J.; Martin, N.; Nelson, J. *J. Chem. Soc., Chem. Commun.* **1995**, 903.

(11) Avecilla, F.; Bastida, R.; de Blas, A.; Fenton, D. E.; Macías, A.; Rodríguez, A.; Rodríguez-Blas, T.; García-Granda, S.; Corzo-Suárez, R. *J. Chem. Soc., Dalton Trans.* **1997**, 409.

(12) Platas, C.; Avecilla, F.; de Blas, A.; Geraldes, C. F. G. C.; Rodríguez-Blas, T.; Adams, H.; Mahía, J. *Inorg. Chem.* **1999**, *38*, 3190.

(13) Geraldes, C. F. G. C.; Zhang, S.; Platas, C.; Rodríguez-Blas, T.; de Blas, A.; Sherry, A. D. *J. Alloys Compd.* **2001**, *323*−*324*, 824.

(14) Platas, C.; Avecilla, F.; de Blas, A.; Rodríguez-Blas, T.; Geraldes, C. F. G. C.; Tóth, É.; Mebach, A. E.; Bünzli, J.-C. G. *J. Chem. Soc., Dalton Trans.* **2000**, 611.

(15) Avecilla, F.; de Blas, A.; Bastida, R.; Fenton, D. E.; Mahía, J.; Macías, A.; Platas, C.; Rodríguez, A.; Rodríguez-Blas, T. *Chem. Commun.* **1999**, 125.

(16) Piguet, C.; Edder, C.; Rigault, S.; Bernardelli, G.; Bünzli, J.-C. G.; Hopfgartner, G. *J. Chem. Soc., Dalton Trans.* **2000**, 3999.

(17) (a) Costes, J.-P.; Dahan, F.; Dupuis, A.; Lagrave, S.; Laurent, J.-P. *Inorg. Chem.* **1998**, *37*, 153. (b) Sanada, T.; Suzuki, T.; Yoshida, T.; Kaizaki, S. *Inorg. Chem.* **1998**, *37*, 4712. (c) Costes, J.-P.; Dahan, F.; Dupuis, A. *Inorg. Chem.* **2000**, *39*, 165. (d) Costes, J.-P.; Dahan, F.; Dupuis, A.; Laurent, J.-P. *Inorg. Chem.* **2000**, *39*, 169. (e) Costes, J.-P.; Dahan, F.; Donnadieu, B.; García-Tojal, J.; Laurent, J.-P. *Eur. J. Inorg. Chem.* **2001**, 363.

(18) (a) Manseki, K.; Kumagai, M.; Sakamoto, M.; Sakiyama, H.; Nishida, Y.; Matsumoto, A.; Sadaoka, Y.; Ohba, M.; Okawa, H. *Bull. Chem. Soc. Jpn.* **1998**, *71*, 379. (b) Casellato, U.; Tamburini, S.; Tomasin, P.; Vigato, P. A. *Inorg. Chim. Acta* **1997**, *262*, 117. (c) Aguiari, A.; Tamburini, S.; Tomasin, P.; Vigato, P. A. *Inorg. Chim. Acta* **1997**, *256*, 199.

(19) (a) Piguet, C.; Bernardelli, G.; Bünzli, J.-C. G.; Petoud, S.; Hopfgartner, G. *J. Chem. Soc., Chem. Commun.* **1995**, 2575. (b) Piguet, C.; Hopfgartner, G.; Williams, A. F.; Bünzli, J.-C. G. *J. Chem. Soc., Chem. Commun.* **1995**, 491.

(20) Piguet, C.; Bünzli, J.-C. G.; Bernardelli, G.; Hopfgartner, G.; Petoud, S.; Schaad, O. *J. Am. Chem. Soc.* **1996**, *118*, 6681.

(21) Piguet, C.; Rivara-Minten, E.; Hopfgartner, G.; Bünzli, J.-C. G. *Helv. Chim. Acta* **1995**, *78*, 1541.

(22) Chen, Q.-Y.; Luo, Q.-H.; Wang, Z.-L.; Chen, J.-T. *Chem. Commun.* **2000**, 1033.

(23) Chen, Q.-Y.; Luo, Q.-H.; Zheng, L.-M.; Wang, Z.-L.; Chen, J.-T. *Inorg. Chem.* **2002**, *41*, 605.

(24) Archibald, S. J.; Blake, A. J.; Parsons, S.; Schröder, M.; Winpenny, R. E. P. *J. Chem. Soc., Dalton Trans.* **1997**, 173.

H, 4.3; N, 13.4. MS-FAB (*m*/*z*): 940 [**2** − NO_3]. IR (KBr): 1633 cm^{-1}. Crystals of the formula [$PrZn(L^1\text{-}3H)(NO_3)](NO_3)\cdot CH_3OH\cdot 0.5CH_3CH_2OH\cdot 0.5H_2O$ suitable for X-ray diffraction were grown by slow diffusion of diethyl ether into a solution of the complex in methanol.

[$NdZn(L^1\text{-}3H)(NO_3)](NO_3)\cdot H_2O$ (3). The yellow complex was prepared as described for **1** by using [$NdL^1(NO_3)](NO_3)_2\cdot 4H_2O$ (0.108 g, 0.1 mmol). Yield: 0.058 g (57%). Anal. Calcd for $C_{39}H_{45}N_{10}NdO_9Zn\cdot H_2O$: C, 45.8; H, 4.6; N, 13.7. Found: C, 45.8; H, 4.4; N, 13.4. Λ_m (Ω^{-1} cm^2 mol^{-1}): 159. MS-FAB (*m*/*z*): 945 [**3** − NO_3]. IR (KBr): 1633 cm^{-1}.

[$SmZn(L^1\text{-}3H)(NO_3)](NO_3)\cdot H_2O$ (4). The yellow complex was prepared as described for **1** by using [$SmL^1(NO_3)](NO_3)_2\cdot 2H_2O$ (0.089 g, 0.084 mmol). Yield: 0.030 g (35%). Anal. Calcd for $C_{39}H_{45}N_{10}O_9SmZn\cdot H_2O$: C, 45.4; H, 4.6; N, 13.6. Found: C, 45.7; H, 4.4; N, 13.4. Λ_m (Ω^{-1} cm^2 mol^{-1}): 183. MS-FAB (*m*/*z*): 951 [**4** − NO_3]. IR (KBr): 1633 cm^{-1}.

[$EuZn(L^1\text{-}3H)(NO_3)](NO_3)\cdot H_2O$ (5). The yellow complex was prepared as described for **1** by using [$EuL^1(NO_3)](NO_3)_2\cdot 3H_2O$ (0.053 g, 0.049 mmol). Yield: 0.029 g (57%). Anal. Calcd for $C_{39}EuH_{45}N_{10}O_9Zn\cdot H_2O$: C, 45.3; H, 4.6; N, 13.6. Found: C, 45.5; H, 4.5; N, 13.4. Λ_m (Ω^{-1} cm^2 mol^{-1}): 146. MS-FAB (*m*/*z*): 952 [**5** − NO_3]. IR (KBr): 1633 cm^{-1}.

[$GdZn(L^1\text{-}3H)(NO_3)](NO_3)\cdot H_2O$ (6). The yellow complex was prepared as described for **1** by using [$GdL^1(NO_3)](NO_3)_2\cdot 3H_2O$ (0.107 g, 0.1 mmol). Yield: 0.050 g (48%). Anal. Calcd for $C_{39}GdH_{45}N_{10}O_9Zn\cdot H_2O$: C, 45.1; H, 4.6; N, 13.5. Found: C, 45.4; H, 4.4; N, 13.3. Λ_m (Ω^{-1} cm^2 mol^{-1}): 195. MS-FAB (*m*/*z*): 957 [**6** − NO_3]. IR (KBr): 1636 cm^{-1}.

[$TbZn(L^1\text{-}3H)(NO_3)](NO_3)\cdot 0.5\ H_2O$ (7). The yellow complex was prepared as described for **1** by using [$TbL^1(NO_3)](NO_3)_2\cdot 2H_2O$ (0.106 g, 0.1 mmol). Yield: 0.041 g (40%). Anal. Calcd for $C_{39}H_{45}N_{10}O_9TbZn\cdot 0.5H_2O$: C, 45.4; H, 4.5; N, 13.6. Found: C, 45.6; H, 4.5; N, 13.4. Λ_m (Ω^{-1} cm^2 mol^{-1}): 177. MS-FAB (*m*/*z*): 958 [**7** − NO_3]. IR (KBr): 1635 cm^{-1}.

[$DyZn(L^1\text{-}3H)(NO_3)](NO_3)\cdot CH_3OH$ (8). The yellow complex was prepared as described for **1** by using [$DyL^1(NO_3)](NO_3)_2\cdot 3H_2O$ (0.108 g, 0.1 mmol). Yield: 0.025 g (24%). Anal. Calcd for $C_{40}DyH_{45}N_{10}O_9Zn\cdot MeOH$: C, 45.4; H, 4.6; N, 13.2. Found: C, 46.7; H, 3.9; N, 13.1. Λ_m (Ω^{-1} cm^2 mol^{-1}): 164. MS-FAB (*m*/*z*): 963 [**8** − NO_3]. IR (KBr): 1636 cm^{-1}.

[$HoZn(L^1\text{-}3H)(NO_3)](NO_3)\cdot H_2O$ (9). The yellow complex was prepared as described for **1** by using [$HoL^1(NO_3)](NO_3)_2\cdot 2.5H_2O$ (0.107 g, 0.1 mmol). Yield: 0.030 g (29%). Anal. Calcd for $C_{39}H_{45}HoN_{10}O_9Zn\cdot H_2O$: C, 44.8; H, 4.5; N, 13.4. Found: C, 45.2; H, 4.2; N, 13.0. Λ_m (Ω^{-1} cm^2 mol^{-1}): 173. MS-FAB (*m*/*z*): 964 [**9** − NO_3]. IR (KBr): 1636 cm^{-1}.

[$ErZn(L^1\text{-}3H)(NO_3)](NO_3)\cdot 2H_2O$ (10). The yellow complex was prepared as described for **1** by using [$ErL^1(NO_3)](NO_3)_2\cdot 2.5H_2O$ (0.107 g, 0.1 mmol). Yield: 0.031 g (29%). Anal. Calcd for $C_{39}ErH_{45}N_{10}O_9Zn\cdot 2H_2O$: C, 44.6; H, 4.5; N, 13.3. Found: C, 44.7; H, 4.2; N, 12.7. Λ_m (Ω^{-1} cm^2 mol^{-1}): 185. MS-FAB (*m*/*z*): 967 [**10** − NO_3]. IR (KBr): 1636 cm^{-1}.

[$TmZn(L^1\text{-}3H)(NO_3)](NO_3)\cdot H_2O$ (11). The yellow complex was prepared as described for **1** by using [$TmL^1(NO_3)](NO_3)_2\cdot 5H_2O$ (0.112 g, 0.1 mmol). Yield: 0.028 g (27%). Anal. Calcd for $C_{39}H_{45}N_{10}O_9TmZn\cdot H_2O$: C, 44.6; H, 4.5; N, 13.3. Found: C, 44.9; H, 4.1; N, 12.9. Λ_m (Ω^{-1} cm^2 mol^{-1}): 172. MS-FAB (*m*/*z*): 968 [**11** − NO_3]. IR (KBr): 1636 cm^{-1}.

[$YbZn(L^1\text{-}3H)(NO_3)](NO_3)\cdot 0.5\ H_2O$ (12). The yellow complex was prepared as described for **1** by using [$YbL^1(NO_3)](NO_3)_2\cdot 0.5H_2O$ (0.109 g, 0.1 mmol). Yield: 0.058 g (56%). Anal. Calcd for $C_{39}H_{45}N_{10}O_9YbZn\cdot 0.5H_2O$: C, 44.8; H, 4.4; N, 13.4. Found: C, 45.0; H, 4.4; N, 13.0. MS-FAB (*m*/*z*): 973 [**12** − NO_3]. IR (KBr): 1637 cm^{-1}. Crystals of the formula [$PrZn(L^1\text{-}3H)(NO_3)](NO_3)\cdot CH_3OH\cdot 2.5H_2O$ suitable for X-ray diffraction were grown by slow diffusion of diethyl ether into a solution of the complex in methanol.

[$LuZn(L^1\text{-}3H)(NO_3)](NO_3)\cdot H_2O$ (13). The yellow complex was prepared as described for **1** by using [$LuL^1(NO_3)](NO_3)_2\cdot 3H_2O$ (0.109 g, 0.1 mmol). Yield: 0.035 g (33%). Anal. Calcd for $C_{39}H_{45}LuN_{10}O_9Zn\cdot H_2O$: C, 44.3; H, 4.5; N, 13.3. Found: C, 44.2; H, 4.1; N, 12.9. Λ_m (Ω^{-1} cm^2 mol^{-1}): 190. MS-FAB (*m*/*z*): 974 [**13** − NO_3]. IR (KBr): 1637 cm^{-1}. Crystals of the formula [$LuZn(L^1\text{-}3H)(NO_3)](NO_3)\cdot 0.5CH_3OH\cdot 0.5H_2O$ suitable for X-ray diffraction were grown by slow diffusion of diethyl ether into a solution of the complex in methanol.

[$YZn(L^1\text{-}3H)(NO_3)](NO_3)\cdot 0.5\ H_2O\cdot 0.5CH_3OH$ (14). The yellow complex was prepared as described for **1** by using [$YL^1(NO_3)](NO_3)_2\cdot 4H_2O$ (0.085 g, 0.083 mmol). Yield: 0.024 g (30%). Anal. Calcd for $C_{39}YH_{45}N_{10}O_9Zn\cdot H_2O\cdot 0.5MeOH$: C, 48.6; H, 4.9; N, 14.0. Found: C, 49.3; H, 4.6; N, 14.3. Λ_m (Ω^{-1} cm^2 mol^{-1}): 143. MS-FAB (*m*/*z*): 888 [**14** − NO_3]. IR (KBr): 1636 cm^{-1}.

[$Zn_2(L^1\text{-}3H)](NO_3)\cdot 3H_2O$ (15). A 0.130 g amount of ligand L^4 (0.22 mmol) was dissolved in 150 mL of ethanol and 92 μL of triethylamine (0.66 mmol) was added. The resultant solution was stirred at room temperature for 48 h, and then stirred and heated to reflux while a solution of 0.065 g of $Zn(NO_3)_2\cdot 6H_2O$ (0.22 mmol) in ethanol (50 mL) was slowly added. The resultant solution was refluxed for 4 h, then concentrated to 30 mL, and finally left to evaporate slowly at room temperature to give complex **15** as yellow crystals. Yield: 0.040 g (40%). Anal. Calcd for $C_{39}H_{45}N_9O_6Zn_2\cdot 3H_2O$: C, 50.9; H, 5.6; N, 13.7. Found: C, 51.2; H, 5.3; N, 13.6. MS-FAB (*m*/*z*): 805 [**15** − NO_3]. IR (KBr): 1633 cm^{-1}. ^1H NMR in DMSO-d_6: δ 2.18 (9H, s), 2.63 (12H, t), 3.01 (12H, t), 7.19 (6H, s), 8.33 (6H, s). ^{13}CNMR in DMSO-d_6: 19.88 (primary C); 57.86, 59.95 (secondary C); 139.60, 171.24 (ternary C); 120.86, 121.33, 167.15 (quaternary C). Crystals of the formula [$Zn_2(L^1\text{-}3H)](NO_3)\cdot H_2O$ suitable for X-ray diffraction were grown by slow evaporation of an ethanolic solution of the complex at room temperature.

Methods. Elemental analyses were carried out on a Carlo Erba 1180 elemental analyzer and FAB-MS spectra were recorded on a FISONS QUATRO mass spectrometer with a Cs ion-gun with 3-nitrobenzyl alcohol as the matrix. ^1H and ^{13}C spectra were run on Bruker AC 200 F or Varian INOVA-300 spectrometers operating at 200 and 300 MHz, respectively. Longitudinal ^1H relaxation times T_1 were measured by the inversion−recovery pulse sequence. IR spectra were recorded, as KBr disks, with a Bruker Vector 22 spectrophotometer. Conductivity measurements were carried out at 20 °C with a Crison Micro CM 2201 conductimeter, using 10^{-3} M solutions of the complexes in acetonitrile. Electronic spectra in the UV−vis range were recorded at 20 °C on a Perkin-Elmer Lambda 900 UV−Vis or Uvikon 942 Plus spectrophotometer, using 1.0 cm quartz cells. Reflectance spectra were recorded as finely ground powders dispersed in MgO (5%) with MgO as reference on a Perkin-Elmer Lambda 900 spectrometer equipped with a PELA-1000 integration sphere.

Luminescence Measurements. Broad band excitation of the finely powdered samples was achieved by a Zeiss XBO 450 W xenon high-pressure lamp coupled with a Zeiss M-20 monochromator. Selective excitation of the Eu(III) $^5D_0$ level was accomplished by a tunable Coherent CR-599 dye laser (band path 0.03 nm, 50−300 mW) pumped by a continuous Coherent Innova-90 argon laser (8 W). Light was conducted to the samples by Oriel liquid optical fibers of 100 cm length, 5 mm o.d. (Xe lamp) or 200 cm length, 3

Table 1. Crystal Data and Structure Refinement for **2**, **12**, **13**, and **15**

	2	**12**	**13**	**15**
formula	$C_{40}H_{54}N_{10}O_{12.5}PrZn$	$C_{40}H_{54}N_{10}O_{12.5}YbZn$	$C_{40}H_{54}LuN_{10}O_{12.5}Zn$	$C_{39}H_{47}N_9O_7Zn_2$
M	1081.21	1113.34	1115.27	884.60
cryst syst	monoclinic	monoclinic	monoclinic	triclinic
space group	$C2/c$	$C2/c$	$C2/c$	$P\bar{1}$
T/K	150(2)	173(2)	150(2)	173(2)
a/Å	33.435(11)	33.154(2)	33.002(10)	13.247(4)
b/Å	10.974(4)	11.0195(8)	10.984(3)	13.291(4)
c/Å	25.842(8)	25.6935(18)	25.501(8)	13.503(4)
α/deg				91.213(7)
β/deg	105.213(7)	104.425(2)	104.626(6)	97.834(6)
γ/deg				119.284(6)
V/Å^3	9150(5)	9091.0(11)	8944(5)	2043.5(10)
F_{000}	4424	4512	4520	920
Z	8	8	8	2
D_{calcd}/g cm^{-3}	1.570	1.627	1.656	1.438
μ/mm^{-1}	1.649	2.645	2.805	1.233
R_{int}	0.0868	0.1146	0.1044	0.1278
no. measd reflns	27167	31410	26365	14739
no. obsd reflns	5914	6177	5652	2920
goodness-of-fit on F^2	0.939	0.926	0.951	0.889
R_1[a]	0.0577	0.0528	0.0582	0.0877
wR_2(all data)[a]	0.1774	0.1252	0.1653	0.2586

[a] $R_1 = \sum||F_o| - |F_c||/\sum|F_o|$; $wR_2 = \{\sum[w(|F_o|^2 - |F_c|^2|)^2]/\sum[w(F_o^4)]\}^{1/2}$.

mm o.d. (laser). The emitted light was analyzed at 90° with a Spex 1404 double monochromator with holographic gratings (band path used 0.01−0.2 nm). Light intensity was measured by a RCA 31034 photomultiplier with a cooled S-20 photocathode (−20 °C), coupled to a Lecroy linear amplifier (500 MHz) and a Stanford Research SR-400 double photon counter. The spectra were transferred into a PC and corrected for the instrumental function. For the lanthanide ions emitting in the near-infrared, light intensity was measured by a Jobin Yvon DSS−IGA020L solid-state InGaAs detector cooled to 77 K, in a LN2 housing including an elliptical mirror (90° beam path, range 800−1600 nm) and coupled to a Jobin Yvon SpectrAcq2 data acquisition system. Luminescent lifetimes were measured with an OPOTEK Vibrant 355 I tunable laser system including a Quantel Brillant Nd:YAG laser (330 mJ at 1064 nm) equipped with frequency doubler (160 mJ at 532 nm), tripler (110 mJ at 355 nm), quadrupler (54 mJ at 266 nm), and a MagicPrism OPO crystal (line width 2−15 cm^{-1}, 25−54 mJ from 410 to 690 nm and 2−12 mJ from 720 to 2400 nm) pumped at 355 nm. Lifetimes obtained by selective excitation of the Eu(III) $^5D_0$ level were measured with a Lambda-Physik-FL3002 pulsed dye laser (1−55 mJ/pulse) pumped at 532 nm. Light was conducted to the samples by an Oriel 77519 Vis-NIR or an Oriel 77514 UV−vis optical laser fiber (460 mm length, 1 mm o.d). The output signal of the photomultiplier was fed into a Standford Research SR-430 multichannel scaler and transferred to a PC. Lifetimes are averages of at least 3 independent determinations. Low-temperature measurements were performed with the help of a CTI−Cryogenics Cryodyne M-22 closed-cycle refrigerator controlled by a Lakeshore 321 temperature controller. Ligand excitation and emission spectra were recorded on a Perkin-Elmer LS-50B spectrometer equipped for low temperature (77 K) measurements. Absolute quantum yields were calculated relative to quinine sulfate in dilute sulfuric acid (absolute quantum yield: 0.546)[25] or cresol violet (absolute quantum yield: 0.52).[26]

X-ray Crystallography. The crystal structure experimental specifications and refinement data are given in Table 1. Three-dimensional, room-temperature X-ray data were collected in the θ ranges 1.26−28.38° (**2**), 1.27−28.28° (**12**), 1.28−28.29° (**13**), and 1.77−28.37° (**15**) on Siemens Smart 1000 CCD (**2** and **13**) or Bruker Smart 1000 CCD (**12** and **15**) instruments. Reflections were measured from a hemisphere of data collected from frames each of them covering 0.3° in ω. Of the 27 167 (**2**), 31 410 (**12**), 26 365 (**13**), and 14 739 (**15**) reflections measured, all of which were corrected for Lorentz and polarization effects and for absorption by multiscan methods based on symmetry-equivalent and repeated reflections, 5914 (**2**), 6177 (**12**), 5652 (**13**), and 2920 (**15**) independent reflections exceeded the significance level ($|F|/\sigma|F|$) > 4.0. The structures were solved by direct methods and refined by full matrix least squares on F^2. Hydrogen atoms were included in calculated positions and refined in the riding mode. Refinement was performed with allowance for thermal anisotropy of all non-hydrogen atoms in **2**, **12**, and **13**. The crystal of **15** presents a slight disorder on the ionic nitrate. This disorder has been resolved and two atomic sites for each of the nitrate atoms have been observed and refined with isotropic atomic displacement parameters in each case. The sites occupancy factors were 0.52721 for N(9), O(1), O(2), and O(3) and 0.47279 for N(9A), O(1A), O(2A), and O(3A). Minimum and maximum final electronic densities of −1.103 and 2.121 e Å^3 for **2** (next to O(1w)), −0.795 and 1.329 e Å^3 for **12** (next to O(1w)), −2.235 and 1.879 e Å^3 for **13** (next to Lu(1)), and −0.567 and 1.137 e Å^3 for **15** were found. Complex scattering factors were taken from the program package SHELXTL[27] as implemented on a Pentium computer.

Results and Discussion

The complexes of the formula $[LnZn(L^1\text{-}3H)(NO_3)](NO_3)\cdot xH_2O\cdot y$MeOH (Ln = Ce to Lu except Pm, $x = 0-2$, $y = 0-1$) were prepared from the corresponding mononuclear $[LnL^1(NO_3)](NO_3)_2\cdot xH_2O$ cryptates, as described in the Experimental Section, in moderate yields (11−58%). The infrared spectra of the complexes (KBr pellets) display an intense absorption band at ca.1635 cm^{-1} attributable to the ν(C=N)$_{imine}$ stretching frequency. This band is shifted ca.

(25) Meech, S. R.; Philips, D. J. *J. Photochem.* **1983**, *23*, 193.
(26) Magde, D.; Brannon, J. H.; Cremers, T. L.; Olmsted, J. *J. Phys. Chem.* **1979**, *83*, 696.
(27) Sheldrick, G. M. SHELXTL Bruker Analytical X-ray System, release 5.1; Madison, WI, 1997.

15 cm^{-1} to lower wavenumbers compared to the mononuclear $[LnL^1(NO_3)](NO_3)_2 \cdot xH_2O$ cryptates.[12] Further evidence for the formation of the heterobinuclear cryptates comes from the FAB mass spectra in which an intense peak corresponding to $[LnZn(L^1\text{-}3H)(NO_3)]^+$ appears in all cases.

In an attempt to prepare the Zn(II) complex with the podand L^4 (Scheme 1) we have obtained the homobimetallic cryptate with the formula $[Zn_2(L^1\text{-}3H)](NO_3)\cdot 3H_2O$ (**15**). It is noteworthy that, although the molar ratio (1:3:1 tren:phenoldicarboxaldehyde:Zn(II); tren = tri(2-aminoethyl)amine) used in the experimental procedure is unfavorable for the formation of the dinuclear cryptate, the system tends to self-organize to produce the bimetallic Zn(II) cryptate, which is obtained in moderate yield (40%). The presence in the IR spectrum of a band at 1633 cm^{-1} attributable to the $\nu(C{=}N)_{imine}$ stretching frequency together with the absence of the band due to the $\nu(C{=}O)$ of the carbonyl indicates the formation of the cryptate, which is confirmed by the presence of an intense peak in the FAB mass spectra corresponding to $[Zn_2(L^1\text{-}3H)]^+$, and by X-ray analysis.

X-ray Structures: Complexes 2, 12, and 13. Crystals of **2**, **12**, and **13** consist of the cations $[LnZn(L^1\text{-}3H)(NO_3)]^+$ (Ln(III) = Pr(III), Yb(III), and Lu(III), respectively) and one well-separated nitrate anion; crystal lattices also contain solvent and water molecules. Figure 1 shows the molecular structure and labeling scheme for the cations. Table 2 and Table S1 (Supporting Information) list selected bond lengths and angles for the metal coordination environment, respectively. In every complex cation, $[LnZn(L^1\text{-}3H)(NO_3)]^+$, the Ln(III) and Zn(II) ions are placed at opposite ends of the cryptand cavity at a very short distance: 3.3252(13) Å for **2**, 3.2925(9) Å for **12**, and 3.2699(14) Å for **13**. These distances are ca. 0.15 Å shorter than the Ln(III)−Ln(III) distances found in the bimetallic cryptates with the formula $[Ln_2(L^1\text{-}3H)(NO_3)_2](NO_3)$ (Ln = Yb, Lu) [Yb−Yb, 3.4444(4) Å; Lu−Lu, 3,447(1) Å],[15] but slightly longer than the Dy(III)−Cu(II) distance reported for $[DyCu(L^2\text{-}3H)(DMF)](ClO_4)_2\cdot MeCN$ (3.255 Å).[22] In the three structures, the Zn(II) ion is hexacoordinated, being bound to three imino-nitrogen atoms, N(2), N(3), and N(4), and the three μ-phenolate oxygen atoms, O(4), O(5), and O(6). The Zn(1)−N(1) distances amount to 3.082 (**2**), 3.083 (**12**), and 3.123 Å (**13**), and they are too long to be considered bond distances. The lanthanide(III) ion is bound to one of the bridgehead nitrogen atoms, N(8), the other three imino-nitrogen atoms, N(5), N(6), and N(7), and the three μ-phenolate oxygen atoms. One or two oxygen atoms of a mono- (**12** and **13**) or bidentate (**2**) nitrate anion occupy the remaining coordination positions. All the Ln(III)−donor atom distances are similar or even shorter than those found in the corresponding homobinuclear 4f−4f cryptates.[15] As previously found in mono- and/or homobinuclear lanthanide(III) analogous cryptates,[12−14] the distance between the corresponding lanthanide(III) ion and the bridgehead nitrogen atom N(8) is considerably longer than those between the lanthanide ion and the imino-nitrogen atoms, showing a weak interaction between the amine nitrogen atom and the Ln(III) ion. The macrobicyclic receptor adopts an *sss endo-*

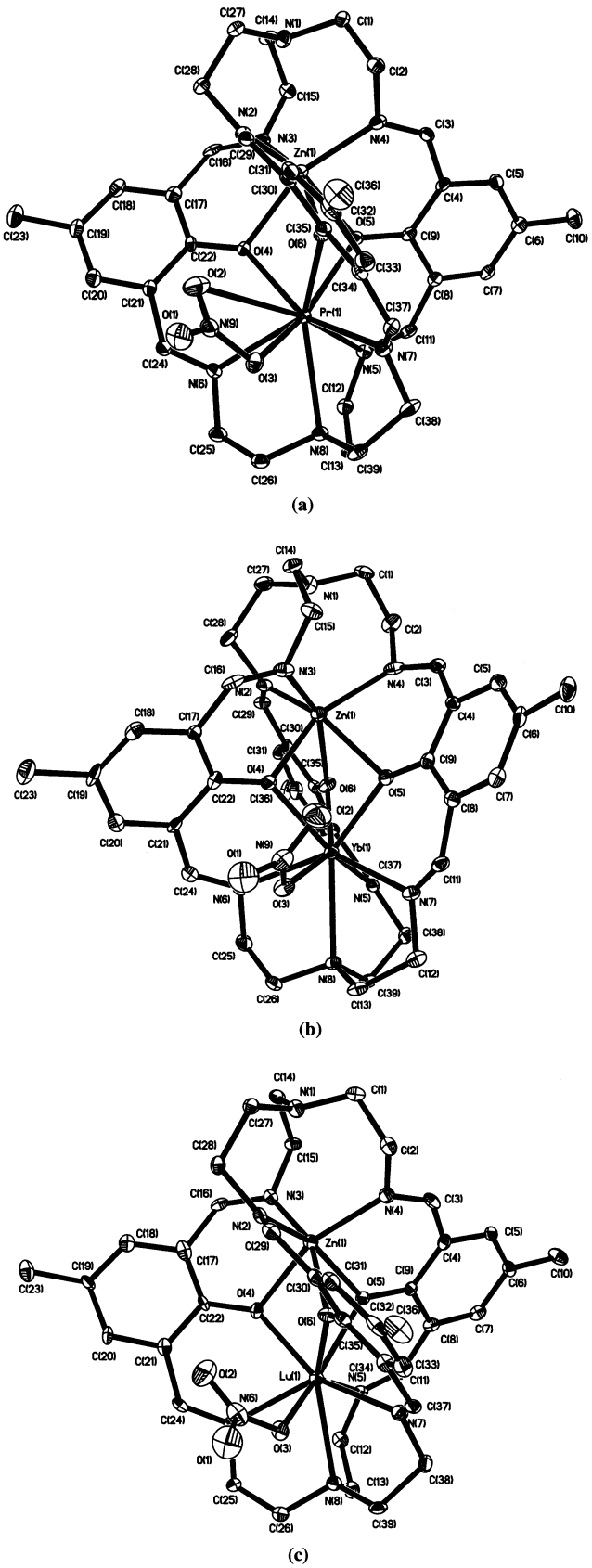

Figure 1. Molecular structures of $[LnZn(L^1\text{-}3H)(NO_3)]^+$: (a) Ln = Pr (**2**) (Λ optical isomer); (b) Ln = Yb (**12**) (Δ optical isomer); (c) Ln = Lu (**13**) (Λ optical isomer). Hydrogen atoms are omitted for simplicity. The ORTEP plot is at the 30% probability level.

Table 2. Selected Bond Lengths (Å) for Complexes **2**, **12**, and **13**

	2	**12**	**13**
Ln−O(4)	2.322(4)	2.235(4)	2.208(6)
Ln−O(6)	2.338(5)	2.345(5)	2.223(6)
Ln−O(5)	2.456(5)	2.212(4)	2.324(6)
Ln−O(3)	2.606(5)	2.374(5)	2.352(6)
Ln−N(7)	2.561(6)	2.472(6)	2.416(8)
Ln−N(5)	2.552(6)	2.435(5)	2.431(7)
Ln−N(6)	2.575(6)	2.414(6)	2.459(8)
Ln−N(8)	2.680(6)	2.609(5)	2.596(7)
Ln−O(2)	2.979(7)		
Zn(1)−N(3)	2.108(7)	2.181(6)	2.071(8)
Zn(1)−O(6)	2.182(5)	2.222(4)	2.077(6)
Zn(1)−N(4)	2.108(7)	2.125(6)	2.091(7)
Zn(1)−N(2)	2.137(6)	2.129(6)	2.150(7)
Zn(1)−O(5)	2.194(5)	2.314(5)	2.188(6)
Zn(1)−O(4)	2.335(5)	2.129(5)	2.299(6)

endo conformation, with the nitrogen atoms of the imine bonds pointing at the same side of the aromatic ring in the three chains and the N(1) and N(8) lone pairs directed toward the central cavity, similar to that found for the mono- and/or homobinuclear lanthanide(III) analogous cryptates.[14,15] The corresponding Ln(III) ion lies 0.9489 (compound **2**), 0.8497 (compound **12**), or 0.8317 Å (compound **13**) above the plane formed by N(5), N(6), N(7), and O(3) (deviation from planarity 0.0089, 0.0436, and 0.0493 Å, respectively) and 1.7417 (**2**), 1.6696 (**12**), or 1.6733 Å (**13**) below the plane defined by the three μ-phenolate oxygen atoms, whereas the Zn(II) ion is located 0.9185 (**2**), 0.9418 (**12**), or 0.9427 Å (**13**) below the plane defined by the three azomethine nitrogen atoms N(2), N(3), and N(4), and 1.5746 (**2**), 1.6162 (**12**), or 1.5891 Å (**13**) above the plane defined by the three μ-phenolate oxygen atoms. The macrobicyclic cavity becomes clearly flattened upon decreasing the size of the lanthanide ion, as inferred from the shortening of the distances between the two bridgehead nitrogen atoms [N(1)−N(8) = 9.071 and 8.977 Å for **2** and **13**, respectively) and between each pair of phenolate oxygen atoms (2.60, 2.64, and 2.98 Å for **2** and 2.50, 2.58, and 2.69 Å for **13**).

The coordination polyhedron around the Ln(III) ion can be best described as a distorted dodecahedron, as previously reported for related systems.[14] In complex **2** one oxygen atom of the coordinated nitrate (O(2)) is capping a triangular face of the dodecahedron.

In the three cryptates, the coordination polyhedron around the Zn(II) ions can be described as a distorted octahedron that shares the triangular face defined by the three phenolate oxygen atoms with the polyhedron around the Ln(III) ion

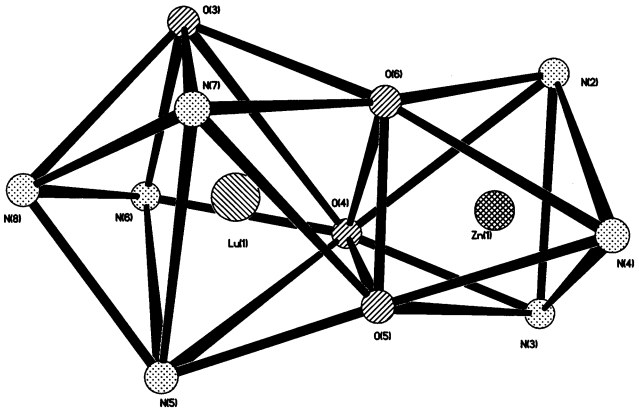

Figure 2. The coordination polyhedra around the Ln(III) and Zn(II) ions in $[LnZn(L^1\text{-}3H)(NO_3)]^+$.

(Figure 2). The twist angles (β) between the triangular faces of the octahedron made up of the three phenolate oxygen atoms (O(4), O(5), and O(6)) and by the three imine nitrogen atoms (N(2), N(3), and N(4)) do not deviate much from the expected values for an octahedron (ideal value 60°), showing a small distortion of the polyhedron around the Zn(II) ion in all cases (Table 3). This is confirmed by the nearly parallel arrangement of these two triangular faces (α, Table 3).

Crystal Structure of 15. Crystals of **15** consist of the cation $[Zn_2(L^1\text{-}3H)]^+$, one well-separated nitrate anion, and a water molecule. Figure 3a displays a view of the cation and gives the atom-labeling scheme and bond lengths for each metal coordination environment. Table S2 (Supporting Information) lists selected bond angles. As expected, both Zn(II) ions are placed into the macrobicyclic cavity, each hexacoordinated bound to three imino-nitrogen atoms and the three μ-phenolate oxygen atoms. The distances between the Zn(II) ions and the bridgehead nitrogen atoms [Zn(1)−N(1) = 3.198 Å and Zn(2)−N(8) = 2.863 Å] are again too long to be considered Zn−N bond distances. The Zn(1) ion lies 1.0251 Å below the plane formed by N(2), N(3), and N(4) and 1.5683 Å above the plane defined by the three μ-phenolate oxygen atoms, whereas the Zn(2) ion is located 0.8298 Å above the plane defined by the three azomethine nitrogen atoms N(5), N(6), and N(7), and 1.5352 Å below the plane defined by the three μ-phenolate oxygen atoms.

In this complex cation the Zn(II) ions are placed at opposite ends of the cryptand cavity at a distance of 3.1037(18) Å. The distance between the two bridgehead nitrogen atoms [N(1)−N(8) = 9.164 Å] is 0.093−0.192 Å

Table 3. Geometric Analysis of the Helical Structures in $[LnZn(L^1\text{-}3H)(NO_3)]^+$ (Ln = Pr (**2**), Yb (**12**), Lu (**13**)) and $[Zn_2(L^1\text{-}3H)](NO_3)$ (**15**) (solid state) and $[YbZn(L^1\text{-}3H)(NO_3)]^+$ in CD_3CN-D_2O (9/1) Solution at 298 K

	2[a]	**12**[a]	**12**[b]	**13**[a]	**15**[a]
α/deg[c]	4.0	3.4	0	3.1	0.3
β[d]	44.9	40.2	45.8	41.53	53.3
					27.8
ϕ/deg	172.3	171.8	180.0	171.5	179.8
mean θ vs_i-R_1/deg	41.1 ± 8.5	40.8 ± 8.3	39.3 ± 0.0	41.0 ± 8.4	36.0 ± 0.1
mean θ vi_i-R_2/deg	36.5 ± 1.68	36.7 ± 0.3	39.0 ± 0.0	36.2 ± 0.42	39.8± 0.17
$\omega_{[vsN(5)-viN(4)]}$	58.2	59.4	69.9	61.0	81.1
$\omega_{[vsN(7)-viN(2)]}$	74.3	60.8	69.9	61.3	81.5
$\omega_{[vsN(6)-viN(3)]}$	55.4	78.6	69.9	80.5	81.7

[a] Solid state. [b] CD_3CN-D_2O (9/1) solution at 298 K. [c] Angle between the two triangular faces of the octahedron around the Zn(II) ions described by O(4), O(5), O(6) and N(2), N(3), N(4). [d] Twist angle of the octahedron around the Zn(II) ions.

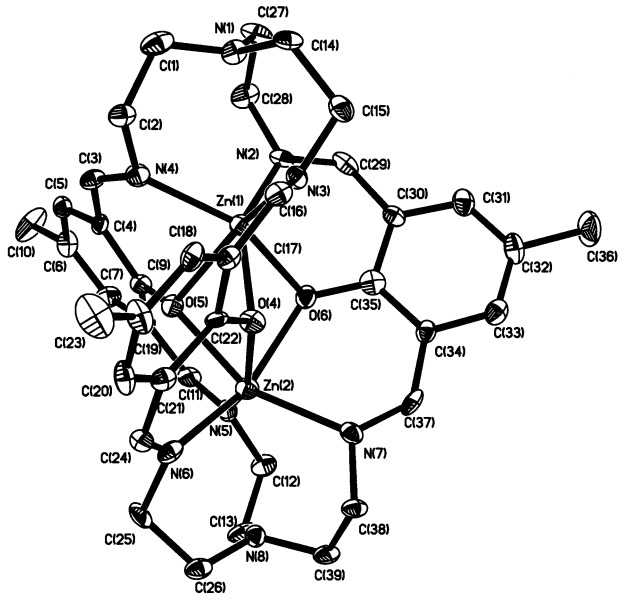

(a)

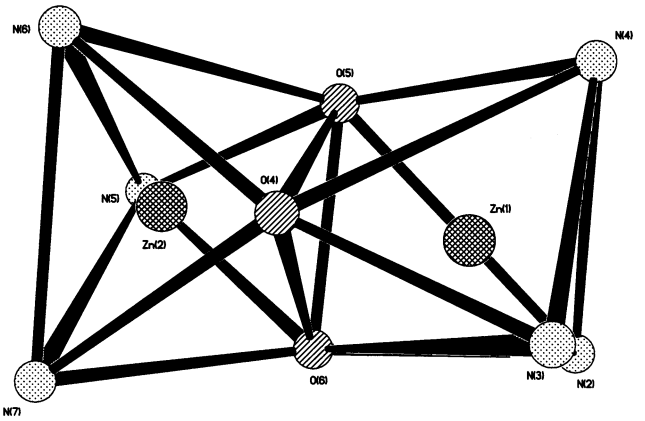

(b)

Figure 3. (a) Molecular structure of $[Zn_2(L^1\text{-}3H)]^+$ in **15**. Hydrogen atoms are omitted for simplicity. Bond lengths (Å) for each metal coordination environment: Zn(1)−N(3) 2.134(8); Zn(1)−O(6) 2.132(6); Zn(1)−N(4) 2.117(8); Zn(1)−N(2) 2.146(8); Zn(1)−O(5) 2.159(6); Zn(1)−O(4) 2.168(7); Zn(2)−O(4) 2.126(6); Zn(2)−O(5) 2.126(6); Zn(2)−O(6) 2.135(7); Zn(2)−N(6) 2.138(9); Zn(2)−N(7) 2.150(8); and Zn(2)−N(8) 2.159(8). The ORTEP plot is at the 30% probability level. (b) The coordination polyhedra around the Zn(II) ions in $[Zn_2(L^1\text{-}3H)]^+$.

longer than that found in **2**, **12**, and **13**, probably because both N(1) and N(8) atoms remain uncoordinated in **15**. The conformation of the ligand in the cryptates can be again described as *sss* and both bridgehead nitrogen atoms are disposed in *endo* orientation.

The coordination polyhedra around both Zn(II) ions can be described as two distorted octahedra which share the face formed by the three phenolate oxygens (Figure 3b). However, the twist angles (β) between the triangular faces described by the three oxygen phenolic atoms and the three imine nitrogen atoms show a very different degree of distortion of the coordination polyhedra around the two Zn ions (Table 3), the one around Zn(1) showing a very strong distortion from an octahedron (ideal value 60°) toward a trigonal prism (ideal value 0°).

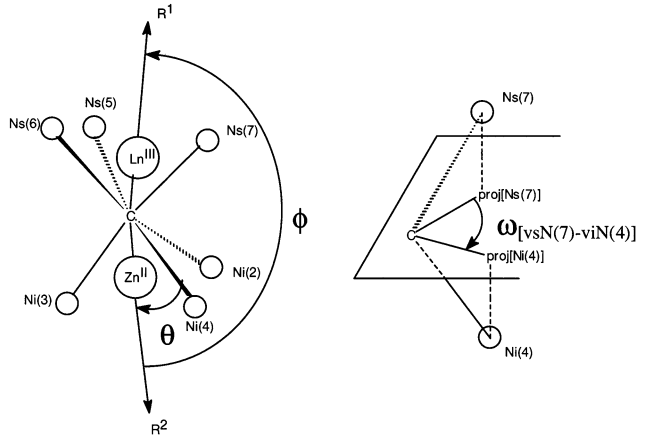

Figure 4. Definition of the angles and vectors used in the analysis of helical structure in complexes **2**, **12**, **13**, and **15**.

Sources of Chirality in the Solid-State Structures of 2, 12, 13, and 15. A remarkable characteristic of this family of compounds is the presence of chirality induced by its triple helical structure. To determine the degree of torsion of the helix around the pseudo C_3 axis, as well as its degree of distortion from the C_3 symmetry, we have analyzed the structures considering the cavity of the cryptand as a trigonal antiprism defined by the six azomethine nitrogen atoms. The upper and lower triangular faces of this antiprism (Figure 4) are connected by the three N═CH−R−CH═N (R = 1,3-(2-OH-5-Me-C_6H_2)) units generating two possible helical structures corresponding to two different optical isomers that can be labeled as Λ or Δ, indicating either *left-handed* (Λ) or *right-handed* (Δ) structural chirality about the pseudo-3-fold symmetry axis of the complex. Thus, we have performed a geometric analysis of the trigonal antiprism based on the determination of three angles, ϕ, θ_i, and ω_i (Figure 4).[28] The average bending of the helical structure is measured by the angle ϕ between the sum vectors R_1 and R_2 ($R_1 = \sum_j C - N_s(j)$, j = 5, 6, and 7; $R_2 = \sum_j C - N_i(j)$, j = 2, 3, and 4; $\phi = 180°$ for an ideal C_3 symmetry and C is a centroid placed in the Ln−Zn axis at equal distance from both metal ions). The angles θ_i reflect the flattening of the helical structure along the pseudo-C_3 axis, defined as $R_2 - R_1$. Finally, the angles ω_i show how much the helix twists along the pseudo-C_3 axis. In **2**, **12**, and **13** the ϕ angles deviate ca. 10° from the expected value of 180° for a symmetrical structure, indicating a small bending of the triple helix along the pseudo-C_3 axis (Table 3). This is confirmed by the almost parallel arrangement of the plane defined by N(2), N(3), and N(4) with that defined by N(5), N(6), and N(7) (ca. 5°). The flattering of the helix along the pseudo-C_3 axis is nearly identical for the three Ln(III)−Zn(II) cryptates, despite the longer Ln(III)−Zn(II) distance observed in **2** compared to **12** and **13**. The analysis of the angles ω_i shows that the individual values deviate significantly from the mean value, reflecting quite distorted helixes. However, these angles clearly point to the helixes becoming more twisted upon decreasing the ionic radius of the Ln(III) ion. The analysis

(28) Elhabiri, M.; Scopelliti, R.; Bünzli, J.-C. G.; Piguet, C. *J. Am. Chem. Soc.* **1999**, *121*, 10747.

Table 4. ^{1}H NMR Shifts (δ, with Respect to TMS), Experimental and Predicted ^{1}H Chemical Shifts of $[YbZn(L^1\text{-}3H)(NO_3)]^+$, Corrected Experimental Longitudinal Relaxation Times (T_1), and Ln···H Distances As Determined in CD_3CN-D_2O (9/1) Solutions at 298 K

	δ_{Lu}^{obs}	δ_{Nd}^{obs}	δ_{Yb}^{obs}	δ_{Yb}^{calc}	δ_{Yb}^{pc}	$\delta_{Yb}^{contact}$	r_i/Å[c]	Nd−T_1/ms	r_i/Å[d]
H_{1ax}	3.80	10.96	−12.01	−11.75			4.14	17.87	3.61
H_{1eq}	3.68	8.85	−10.75	−10.92			4.47	*e*	
H_{2ax}	2.87	8.08	5.25	*b*	3.84	−6.22	3.54	18.87	3.65
H_{2eq}	3.20	8.70	−4.54	*b*	2.09	5.65	4.32	*e*	
H_3	8.26	23.11	9.43	*b*	−6.80	5.63	4.27	66.03	4.49
H_4	7.33	9.40	9.73	11.76			5.60	247.01	5.60
H_5	2.25	2.25	*a*				7.73	1078	
H_6	7.37	8.44	6.23	7.94			6.29	620.3	6.53
H_7	8.36	7.08	4.55	5.32			5.64	366.6	5.98
H_{8ax}	3.38	5.34	−3.87	−3.37			5.50	205.1	5.43
H_{8eq}	3.13	3.99	−1.12	−0.87			6.19	393.4	6.05
H_{9ax}	2.72	3.88	−1.93	−1.16			6.85	594.2	6.48
H_{9eq}	3.03	4.14	−0.65	−0.61			7.35	1062	7.14
D_1			789 ± 19						
D_2			0 ± 56						
AF_j			0.01395						

[a] Not assigned. [b] Not included in the calculation because contact shifts are important (see text). [c] Calculated Yb^{III}···H distances from LIS data. [d] Experimental Nd(III)···H distances obtained according to eq 6 and normalized to the Nd···H_4 distance. [e] Overlapping of H_{1eq} and H_{2eq} prevents an accurate determination of T_1.

of complex **15** reveals a less distorted and more twisted helical structure compared with those of cryptates **2**, **12**, and **13** (Table 3).

Each of the coordinated $N^a-[(CH_2-CH_2)-N^i]_3$ units of the macrobicyclic receptor $(L^1\text{-}3H)^{3-}$ (where N^a and N^i denote the amine and imine nitrogen atoms respectively) forms three five-membered chelate rings $\overline{Ln-N^a-C-C-N^i}$ in compounds **2**, **12**, and **13**, adopting a $(\delta\delta\lambda)_5$ or $(\lambda\lambda\delta)_5$ conformation. Moreover, the three five-membered pseudo-chelate rings $\overline{Zn-N^i-C-C-N^a}$ adopt $(\delta\delta\delta)_5$ or $(\lambda\lambda\lambda)_5$ conformations. In the following, we will use the notations δ' and λ' for the two enantiomeric forms of the five-membered pseudo-chelate rings $\overline{Zn-N^i-C-C-N^a}$. Inspection of the crystal structure data reveals that in **2**, **12**, and **13** two $\Lambda(\delta\delta\lambda)_5(\delta'\delta'\delta')_5$ and $\Delta(\lambda\lambda\delta)_5(\lambda'\lambda'\lambda')_5$ enantiomers cocrystallize in equal amounts (racemate). This $(\lambda\lambda\delta)_5$ or $(\delta\delta\lambda)_5$ "conformational mixture" is probably induced by the presence, in the solid state, of a relatively bulky nitrate anion between two chains of the ligand that makes the symmetric $(\lambda\lambda\lambda)_5$ (or $(\delta\delta\delta)_5$) conformation energetically less favorable than the asymmetric $(\lambda\lambda\delta)_5$ (or $(\delta\delta\lambda)_5$) one. The crystal structure data of **15** show that the two enantiomers present in the crystal are $\Lambda(\delta'\delta'\delta')_5(\delta'\delta'\delta')_5$ and $\Delta(\lambda'\lambda'\lambda')_5(\lambda'\lambda'\lambda')_5$, probably because the absence of the coordinated nitrate ligand render the symmetric structure more stable.

Structure in Solution of the Ln−Zn Cryptates. The structure in solution of the heterobinuclear 4f-Zn complexes was studied by ^{1}H NMR spectroscopy in CD_3CN-D_2O mixtures (9:1), since the solubility of the complexes in water is poor at room temperature. The spectra of the Y−Zn (**14**) and Lu−Zn (**13**) diamagnetic complexes indicate that the systems have an effective C_3 symmetry in solution, with the Ln(III) and Zn(II) ions inside the cavity of the cryptand placed each at one end (see Scheme 2 for the outline solution structure of the complexes and the atom labeling used in the NMR study). The spectra were assigned on the basis of signal intensities and NOESY (0.5 s mixing time) two-

Scheme 2

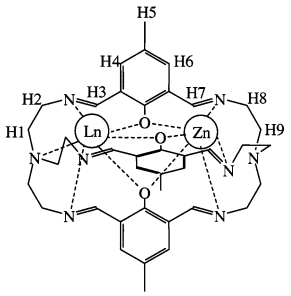

dimensional experiments (Table 4). NOESY cross-peaks were observed between H3/H4, H6/H7, H2/H3, and H7/H8 protons. The effective C_3 symmetry indicates that the complexes possess a somewhat different structure in solution and in the solid state. This is probably due to an intramolecular conversion of one of the three five-membered chelate rings $\overline{Ln-N^a-C-C-N^i}$ ($\delta \rightarrow \lambda$ or $\lambda \rightarrow \delta$), resulting in a complex cation that possesses C_3 symmetry $\Lambda(\delta\delta\delta)_5(\delta'\delta'\delta')_5$ or $\Delta(\lambda\lambda\lambda)_5(\lambda'\lambda'\lambda')_5$ in solution.

For paramagnetic lanthanide complexes, the isotropic paramagnetic chemical shift of a ligand nucleus *i* induced by a lanthanide ion *j* (LIS) consists of contact (δ_{ij}^c) and pseudocontact (δ_{ij}^{pc}) contributions:[3]

$$\delta_{ij}^{para} = \delta_{ij}^{exp} - \delta_i^{dia} = \delta_{ij}^c + \delta_{ij}^{pc} \qquad (1)$$

The diamagnetic component (δ_i^{dia}) can be directly evaluated from the respective shifts of the La(III), Y(III), or Lu(III) complexes. Although both contact and pseudocontact contribution terms potentially provide useful structural information, the δ_{ij}^{pc} term is more widely used because of its direct relationship to structure (eq 2).[3] Here, D_1 is proportional to the magnetic susceptibility difference, $\chi_{zz} - {}^1/_3(\chi_{xx} + \chi_{yy} + \chi_{zz})$, D_2 is proportional to the susceptibility difference

$$\delta_{ij}^{pc} = D_1\left[\frac{3\cos^2\theta - 1}{r^3}\right] + D_2\left[\frac{\sin^2\theta\cos 2\varphi}{r^3}\right] \qquad (2)$$

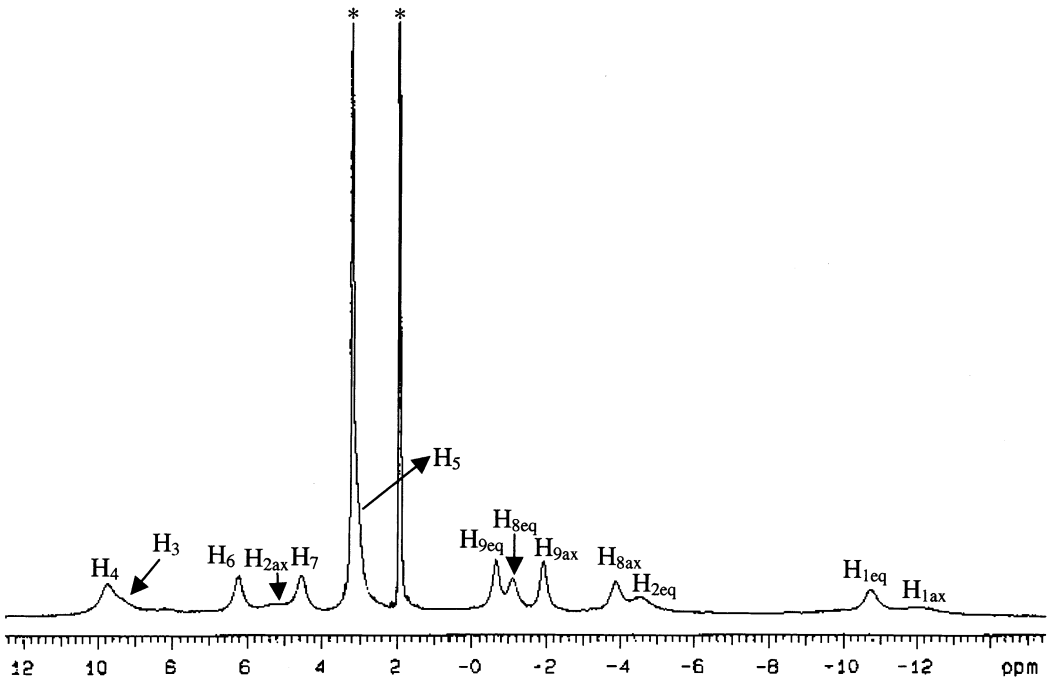

Figure 5. The proton NMR spectrum (300 MHz) of the Yb−Zn cryptate (**12**) in CD_3CN-D_2O (9:1) at 298 K. The asterisk (∗) denotes solvent signals.

$\chi_{xx} - \chi_{yy}$, and θ, φ, and r are the polar coordinates of each nucleus with respect to the highest fold symmetry axis of the Ln(III) complexes. In the case of lanthanide complexes of axial symmetry, eq 2 can be written in the simplified form[29,30]

$$\delta_{ij}^{pc} = C_j G \tag{3}$$

where C_j depends on the Ln^{III} ion and G contains information about crystal field parameters and the position in space of a given nucleus i.

The contact shift is given by[3]

$$\delta_{ij}^{c} = \langle S_z \rangle F = \langle S_z \rangle \frac{\beta}{3kT\gamma_I} \frac{A}{\hbar} 10^6 \tag{4}$$

where $\langle S_z \rangle$ is the reduced value of the average spin polarization, β the Bohr magneton, k the Boltzmann constant, γ_I the gyromagnetic ratio of the nucleus in question, T the absolute temperature, and $A/\hbar$ the hyperfine coupling constant (in rad s^{-1}).

The ^1H NMR spectrum of the Yb−Zn cryptate is shown in Figure 5. The hyperfine ^1H NMR shifts in Yb(III) complexes are considered to be largely pseudocontact in origin, and therefore the observed LIS values may be analyzed directly with eq 2. A full assignment and hyperfine chemical shift analysis was carried out by using the Shift Analysis method described by Forsberg et al.,[31] which requires an initial estimate of the structure. Initially, the atomic coordinates from the X-ray crystal structure of the Yb−Zn cryptate were used to asses the agreement between the experimental and predicted Yb(III) induced shifts. The agreement between the experimental and calculated LIS values was poor ($AF_j = 0.1889$, eq 5), and we obtained D_1 and D_2 values of -457 ± 77 and 896 ± 126 ppm Å^3, respectively. Since D_2 values near zero are expected for complexes with axial symmetry, these results demonstrate that the X-ray structure of the Yb−Zn cryptate is not a good model for the structure of the complex in solution.

$$AF_j = [\sum_i (\delta_{ij}^{exp} - \delta_{ij}^{cal})^2 / \sum_i (\delta_{ij}^{exp})^2]^{1/2} \tag{5}$$

To generate a reasonable model of the structure in solution with a perfect C_3 symmetry we followed a similar procedure to that previously described for lanthanide triple-stranded helical complexes:[32] the Cartesian coordinates corresponding to one of the $N-(CH_2)_2N{=}CH-R-CH{=}N(CH_2)_2-N$ (R = 1,3-(2-OH-5-Me-C_6H_2)) chains were taken from the X-ray structure of the Yb−Zn cryptate (**12**), and the C_3 axis of symmetry of the complex was considered to pass through both bridgehead nitrogen atoms. The Yb(III) and Zn(II) ions were placed onto this axis by fixing the $Yb-N_{bridgehead}$ and Yb(III)−Zn(II) distances to those observed experimentally for **12** in the solid state (2.609 and 3.2925 Å, respectively). This set of Cartesian coordinates was converted into cylindrical (r, θ, z) coordinates, the cylindrical coordinates for the other two chains of the cryptate were calculated assuming trigonal symmetry, and the cylindrical coordinates were transformed back into Cartesian coordinates. These coordinates correspond to a structure that possesses a C_3 symmetry $\Lambda(\delta\delta\delta)_5(\delta'\delta'\delta')_5$ or $\Delta(\lambda\lambda\lambda)_5(\lambda'\lambda'\lambda')_5$.

An agreement factor AF_j of 0.16 was obtained with these coordinates, with the D_1 and D_2 values amounting to 668 ±

(29) Bleaney, B. *J. Magn. Reson.* **1972**, *8*, 91.
(30) Bleaney, B.; Dobson, C. M.; Levine, B. A.; Martin, R. B.; Williams, R. J. P.; Xavier, A. V. J. *J. Chem. Soc., Chem. Commun.* **1972**, 791.
(31) Forsberg, J. H.; Delaney, R. M.; Zhao, Q.; Harakas, G.; Chandran, R. *Inorg. Chem.* **1995**, *34*, 3705.
(32) Platas-Iglesias, C.; Piguet, C.; André, N.; Bünzli, J.-C. G. *J. Chem. Soc., Dalton Trans.* **2001**, 3084.

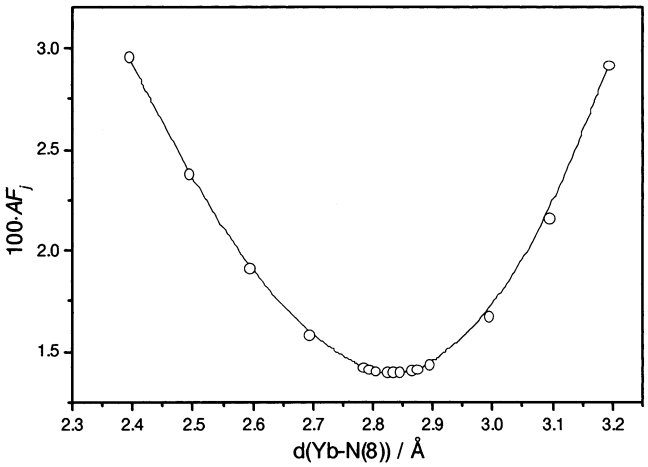

Figure 6. Plot of the agreement factor AF_j vs the Yb−N(8) bond distance for **12** in CD_3CN-D_2O (9/1) solution at 298 K.

51 and 17 ± 130 ppm Å^3, respectively. However, dramatic improvements in the agreement factors were obtained when the protons placed three bonds away from the Yb(III) center H_{2ax}, H_{2eq}, and H_3 were excluded from the fitting procedure. This fact reveals that contact shifts for these protons should not be neglected, as previously observed for Yb(III) texaphyrins[33] and Yb(III) Schiff-base macrocyclic complexes.[34] We therefore excluded these protons from our fitting calculations. The remaining protons were used to estimate the idealized Ln−donor distances with the Shift Analysis program:[31] the Yb(III) ion was moved along the *z* axis, and a plot of the agreement factor AF_j (eq 5) vs the $Yb-N_{bridgehead}$ distance revealed a minimum that best fit the LIS data (Figure 6). The experimental and calculated isotropic shifts are summarized in Table 4. The resulting agreement factor AF_j = 0.01395 is excellent, and the calculated D_1 and D_2 parameters amount to 787 ± 19 and 0 ± 56 ppm Å^3, respectively.

The obtained idealized $Ln-N_{bridgehead}$ distance was 2.83 Å, ca. 0.22 Å longer than that found in the solid state (2.609 Å), while the idealized $Ln-N_{imine}$ and $Ln-O_{phenolate}$ distances were 2.50 and 2.08 Å, respectively, in relative good agreement with the averaged distances found for the Yb−Zn cryptate (**12**) in the solid state (2.44 and 2.26 Å, respectively). The quantitative analysis of the helical structure of **12** in solution performed as described above for the solid-state structures led to values of ϕ, θ_i, and ω_i close to those observed in the solid state (Table 3). These results indicate that the structure of the Yb−Zn cryptate (**12**) in solution is somewhat different from that found in the solid state but the helical structure is maintained. The main difference between the structures in solution and in the solid state corresponds to the conformation of one of the three five-membered chelate rings $Ln-N^a-C-C-N^i$, which changes from the "mixed conformations" $(\delta\delta\lambda)_5$ or $(\lambda\lambda\delta)_5$ in the solid state to $(\delta\delta\delta)_5$ or $(\lambda\lambda\lambda)_5$ in solution.

The calculated D_1 and D_2 parameters (eq 2) were used to determine the dipolar shifts for the omitted H_{2ax}, H_{2eq}, and H_3 protons (Table 4). Subsequently, the contact shifts were obtained by subtracting the calculated dipolar contributions from the measured isotropic shifts. The resulting values, which were found to be substantial, are presented in Table 4.

Among the lighter Ln(III) ions (Ln = Ce → Eu), Nd(III) has the longest electron relaxation times,[35,36] and therefore is frequently used to obtain structural information of lanthanide complexes in solution.[37] The Nd(III)-induced ^1H NMR longitudinal relaxation enhancements for the Nd−Zn cryptate (**3**) have been measured at 7.04 T and 25 °C. To correct for diamagnetic contributions, the relaxation rates for the corresponding Lu−Zn cryptate were subtracted from the measured values of **3** (Table 4). Since it is only for remote nuclei that the outer-sphere contribution ($1/T_{1,OS}$) becomes significant, this contribution was neglected in our study. The effects of the paramagnetic center on T_1 are accounted for by the Solomon−Bloembergen−Morgan theory, which reduces to dipolar and Curie-spin contributions, depending on r_i^{-6}, for lanthanide complexes.[3] The use of a nucleus sufficiently remote from the paramagnetic center as an internal reference gives eq 6,[3] in which k_i^{tot} and k_i^{dia} are the

$$\frac{k_{ref}^{tot} - k_{ref}^{dia}}{k_i^{tot} - k_i^{dia}} = \left(\frac{r_i}{r_{ref}}\right)^6 \qquad (6)$$

longitudinal relaxation rates measured for the nucleus *i* in the paramagnetic complex and its diamagnetic analogue, respectively. Application of this equation allows the determination of relative *r* values in the complexes without the need to have good estimates for the correlation times τ_c for the nuclear−electronic dipolar interaction of the complex, needed to calculate absolute *r* values. These correlation times are T_{1e} (the electronic spin−lattice relaxation time) for the dipolar interaction and τ_R (the rotational correlation time) for the Curie spin contribution (in Ln(III) complexes where Ln ≠ Gd). The long distance from H_5 protons to the Nd(III) ion causes the Nd(III)-induced relaxation rate enhancement effect to be small and the corresponding Nd−H distances to be inaccurate; hence, these data were not considered. The agreement between the experimental Nd···H distances obtained from relaxation data and those determined for Yb(III) in solution from LIS data is satisfactory for all protons except for H_{1ax} (Table 4), indicating that the Nd−Zn (**3**) and Yb−Zn (**12**) cryptates adopt very similar structures in solution.

Photophysical Properties: Ligand-Centered Transitions. Relevant photophysical data are presented in Table 5. The electronic spectra of the cryptates display three regions of absorption: a band centered around 26 400 cm^{-1} typical

(33) Lisowski, J.; Sessler, J. L.; Lynch, V.; Mody, T. D. *J. Am. Chem. Soc.* **1995**, *117*, 2285.
(34) Lisowski, J. *Magn. Reson. Chem.* **1999**, *37*, 287.
(35) Alsaadi, B. M.; Rossotti, F. J. C.; Williams, R. J. P. *J. Chem. Soc., Dalton Trans.* **1980**, 2151.
(36) Bertini, I.; Capozzi, F.; Luchinat, C.; Nicastro, G.; Xia, Z. *J. Phys. Chem.* **1993**, *97*, 6351.
(37) Lammers, H.; Maton, F.; Pubanz, D.; van Laren, M. W.; van Bekkum, H.; Merbach, A. E.; Muller, R. N.; Peters, J. A. *Inorg. Chem.* **1997**, *36*, 2527.

Table 5. Ligand-Centered Absorption and Emission Properties (cm^{-1}) of $[LnZn(L^1\text{-}3H)(NO_3)]^+$

compd	$\pi \rightarrow \pi^*$ [a]	$\pi \rightarrow \pi^*$ [b]	$^1\pi\pi^*$ [c]	$^3\pi\pi^*$	$\tau(^3\pi\pi^*)$
Nd	26 387 (4.34)	25 640	*f*	*f*	
	39 692 (4.93)	34 453			
	46 079 (4.92)	45 361			
Eu	26 387 (4.36)	25 646	22 779	*f*	
	39 791 (4.95)	34 451			
	46 087 (4.93)	45 358			
Gd	26 453 (4.44)	25 642	22 421	18 248−17 271[d]	1.63(9)[d]
	39 841 (5.03)	34 445		20 121−18 904[e]	1.57(7)[e]
	46 145 (5.01)	45 358			
Tb	26 458 (4.34)	25 646	*f*	*f*	
	39 811 (4.94)	34 453			
	46 183 (4.91)	45 358			
Lu	26 110 (4.33)	25 640	22 272	18 692−17 271[d]	
	40 000 (4.94)	34 457		20 367−18 553[e]	
	46 083 (4.91)	45 358			

[a] Electronic spectral data in acetonitrile at 295 K; energies are given for the maximum of the band envelope in cm^{-1}, and log ϵ is given within parentheses. [b] Reflectance spectra recorded at 295 K. [c] Luminescence data in acetonitrile at 295 K. [d] Luminescence data and lifetimes (ms) in the solid state at 77 K. [e] Luminescence data and lifetimes (ms) in frozen acetonitrile solution at 77 K. [f] Luminescence quenched by transfer to the lanthanide ion.

of polyazamacrocycles, assigned to the C═N chromophores,[38] a band at ca. 39 800 cm^{-1} arising from transitions located on the substituted phenol moieties, and an intense absorption around 46 000 cm^{-1}. The emission spectra of the Gd−Zn (**6**) and Lu−Zn (**13**) cryptates in acetonitrile solution (295 K) under excitation through the ligand bands present a single band centered at ca. 22 300 cm^{-1} (Table 5) whose intensity quickly diminishes when a short delay (0.1 ms) is enforced and therefore has been attributed to the $^1\pi\pi^*$ state. The absolute fluorescence quantum yield is low and amounts to $Q = 0.24\%$ for **6** and 0.36% for **13**, compared to 0.2% for the monometallic cryptate.[14] The emission spectra recorded in frozen acetonitrile solutions at 77 K present a second more structured band (Figure 7). These bands have a single-exponential time decay with lifetimes of ca. 1.6 ms and are therefore assigned to the $^3\pi\pi^*$ state. The energy of the ligand $^3\pi\pi^*$ emission changes dramatically when the emission spectrum is recorded in the solid state (Figure 7), the energy of the $^3\pi\pi^*$ 0-phonon transition lying 1873 cm^{-1} below the position observed in frozen acetonitrile solution. This suggests that the structure of the cryptates is different in the solid state and in solution, in agreement with the ^{1}H NMR data (vide supra). The luminescence of the ligand $^3\pi\pi^*$ state is completely quenched in the Eu−Zn and Tb−Zn cryptates at low temperature (Figure 7), while the characteristic emission bands of Eu(III) and Tb(III) appear, pointing to sensitization of the metal ions via a ligand-to-metal energy transfer.

Photophysical Properties of the Eu−Zn and Tb−Zn Cryptates. A high-resolution study has been performed on solid samples of the Eu−Zn (**5**) and Tb−Zn (**7**) cryptates to gain information on the chemical environment of the metal ion. The excitation spectrum of a solid sample of **5** at 10 K produces a broad and intense band with a maximum at 24 390 cm^{-1}, assigned to excitation through the $^1\pi\pi^*$ ligand

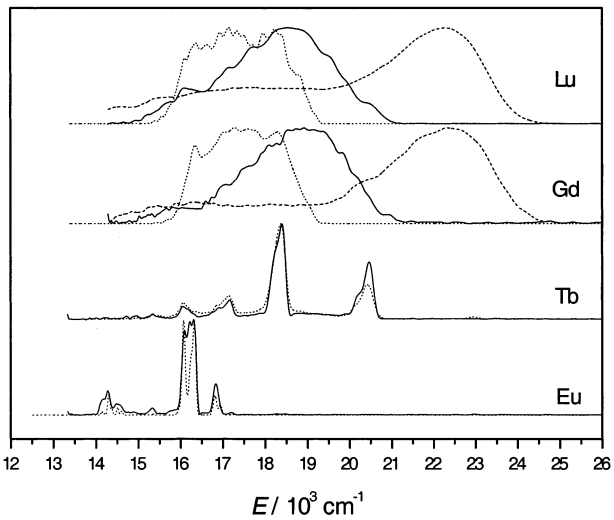

Figure 7. Corrected phosphorescence spectra of the Ln−Zn cryptates at 77 K in the solid state (dotted lines), corrected phosphorescence spectra of the Ln−Zn cryptates in frozen acetonitrile solution (solid lines), and fluorescence spectra of the Gd−Zn and Lu−Zn cryptates in acetonitrile solution at 295 K (dashed lines). Vertical scale: arbitrary units.

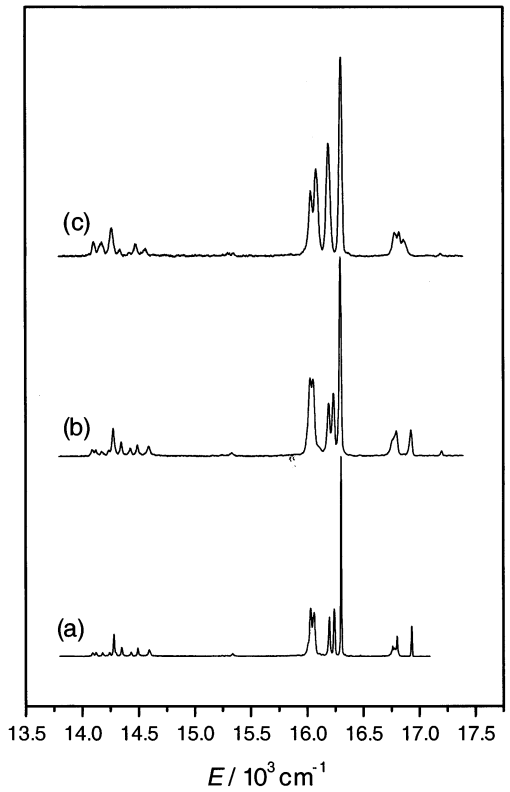

Figure 8. Corrected emission spectra of the Eu−Zn cryptate (**5**) at 10 K: (a) $\nu_{exc} = 17\,206$ cm^{-1}, solid state; (b) $\nu_{exc} = 23\,866$ cm^{-1}, solid state; and (c) 10^{-4} M in CH_3CN, $\nu_{exc} = 25\,253$ cm^{-1}. Vertical scale: arbitrary units.

state. The corresponding emission spectrum displays the characteristic Eu($^5D_0 \rightarrow {}^7F_J$) transitions (Figure 8). Upon broad-band excitation at 10 K, the integrated and corrected relative intensities of the $^5D_0 \rightarrow {}^7F_J$ transitions are 0.08, 1.00, 5.77, 0.14, and 1.60 for $J = 0$, 1, 2, 3, and 4, respectively. The high-resolution excitation spectrum in the $^5D_0 \leftarrow {}^7F_0$ range obtained by analyzing the maximum on the $^5D_0 \rightarrow {}^7F_2$ transition at 10 K displays a single sharp and symmetrical

(38) Aruna, V. A. J.; Alexander, V. *J. Chem. Soc., Dalton Trans.* **1996**, 1867.

Table 6. Energy (cm^{-1}) of the $^5D_0$ and of the Identified ^7F_J Crystal Field Sublevels (origin: $^7F_0$) in the $[EuZn(L^1\text{-}3H)(NO_3)](NO_3)\cdot H_2O$ (**5**) Cryptate from Luminescence Spectra at 10 K in the Solid State and in Frozen Acetonitrile Solution

				Solid					
$^5D_0$	17 205	$^7F_1$	279	$^7F_2$	909	$^7F_3$	1875	$^7F_4$	2616
			412		971				2716
			446		1013				2780
					1152				2860
					1177				2931
									2970
									3032
									3086
									3116
				10^{-4} M in MeCN					
	17 197		336		896		1849		2634
			376		1006				2725
			417		1116				2778
					1164				2861
									2936
									3022
									3095

peak at 17 208 cm^{-1} with a full width at half-height (fwhh) of 4.7 cm^{-1}, typical of a well-defined coordination site. However, it also displays a shoulder on the high-energy side. Analyzing on the other components of the $^5D_0 \rightarrow {}^7F_2$ or $^5D_0 \rightarrow {}^7F_4$ transitions reveals an identical excitation spectrum, indicating that vibronic transitions are responsible for the additional shoulder at 17 205 cm^{-1} appearing in the excitation spectra.[14] The emission spectra may be interpreted in terms of the presence of a single, low-symmetry Eu(III) site, since the transitions to $^7F_2$ and $^7F_4$ display five and nine components, respectively. The transition to the $^7F_1$ level contains more than the expected ($2J + 1$) components, but a correlation between the infrared and luminescence spectra clearly demonstrates that the transition contains a vibronic component (427 cm^{-1}). A similar situation was observed for the mononuclear $[EuL^1(NO_3)](NO_3)_2$ cryptate.[14] Electronic sublevels of the ^7F_J ($J = 1-4$) manifold are reported in Table 6.

The excitation spectrum of the Eu−Zn cryptate (**5**) recorded from a frozen acetonitrile solution at 10 K produces a broad band with a maximum at 24 390 cm^{-1}, corresponding to the excitation through the $^1\pi\pi^*$ ligand state. The corresponding emission spectrum displays the characteristic Eu($^5D_0 \rightarrow {}^7F_J$) transitions (Figure 8). The integrated and corrected relative intensities of the $^5D_0 \rightarrow {}^7F_J$ transitions are 0.12, 1.00, 5.44, 0.21, and 1.44 for $J = 0$, 1, 2, 3, and 4, respectively. The spectrum presents some important differences with respect to that recorded in the solid state (Figure 8), since the transitions to $^7F_4$ and $^7F_2$ display only seven and four components and the energy of the electronic sublevels of the ^7F_J ($J = 1-4$) manifold is different (Table 6). This points again to the Eu−Zn cryptate having a somewhat different Eu(III) chemical environment in solid state and in solution, in agreement with the ^{1}H NMR data (vide supra).

At low temperature, the lifetimes of the Eu($^5D_0$) level (Table 7) are in the range 800−870 (solid state) and 700−850 μs (acetonitrile). The emission spectra recorded at room temperature both in the solid state and in solution result in a very weak emission. Moreover, upon increasing the temperature, the lifetime becomes considerably shorter, which is indicative of a temperature-dependent quenching mechanism such as mixing with ligand vibrational modes or back transfer to the $^3\pi\pi^*$ state of the ligand. Reinhoudt and co-workers[39] have concluded from their work on modified Eu(III)-containing calix[4]arenes that the antenna effect is maximum when the $^3\pi\pi^*$ 0-phonon transition lies 3500 cm^{-1} above the lanthanide excited state. They also observed that the $^1\pi\pi^* \rightarrow {}^3\pi\pi^*$ intersystem crossing is maximized when the energy difference between these states amounts to ca. 5000 cm^{-1}. A similar conclusion was reached by Latva et al.,[40] finding that the best efficiency in energy transfer is obtained when the 0-phonon band of $^3\pi\pi^*$ lies at 21 000−22 000 cm^{-1}. In the case of the Eu−Zn cryptate (**5**), we note that the 0-phonon transition of the ligand $^3\pi\pi^*$ state (as measured for the gadolinium complex) lies at 18 248 (solid state) and 20 121 cm^{-1} (frozen solution), leading to $\Delta E(^3\pi\pi^* - {}^5D_0)$ differences equal to 1051 and 2916 cm^{-1}, respectively. Moreover, the $^1\pi\pi^* - {}^3\pi\pi^*$ energy difference (as measured for the gadolinium complex in acetonitrile solution) amounts to 3347 cm^{-1}. These data clearly explain the poor sensitization of Eu(III) at room temperature and the longer lifetimes observed at 295 K in acetonitrile solution (348 μs) compared with those obtained in solid-state samples (57−92 μs). However, the presence of a quenching effect by a ligand-to-metal charge transfer[41] state cannot be ruled out either, but we are unable to evidence a LMCT (ligand-to-metal charge-transfer band) transition in the absorption spectrum of **5**. Upon addition of H_2O or D_2O up to a concentration of 0.25 M to a 10^{-4} M acetonitrile solution of the complex at 295 K the lifetimes of the Eu($^5D_0$) level (Table 7) remain unchanged, indicating that the coordinated nitrate anion is not replaced by water molecules under these conditions. The quantum yield of the metal-centered luminescence in the Eu−Zn cryptate amounts to 1.05% upon

Table 7. Lifetimes of the Eu($^5D_0$) and Tb($^5D_4$) Excited Levels (μs) in $[LnZn(L^1\text{-}3H)(NO_3)]^+$ Complexes in Solid-State Samples and Solutions under Various Excitation Conditions

compd	conditions	T/K	ν_{exc}/cm^{-1}	ν_{an}/cm^{-1}	τ_f/μs
5 (Ln = Eu)	solid	10	17 208	16303	791(3)
			28 169		867(2)
		295	17 216	16308	57(4)
			28 169		92(2)
	10^{-4} M in CH_3CN	10	28 169	16301	856(1)
			21 468		693(2)
		295	28 169	16308	348(5)
			21 468		345(9)
	10^{-4} M in	295	24 096	16306	382(3)
	$CD_3CN + D_2O$[a]		21 468		353(1)
	10^{-4} M in	295	24 096		388(3)
	$CH_3CN + H_2O$[a]		21 468		374(1)
7 (Ln = Tb)	solid	10	28 169	18397	849(3)
			20 377		827(4)
	10^{-4} M in CH_3CN	10	28 169	18371	1053(3)
			20 381		1063(5)

[a] 2.5×10^{-1} M of D_2O (or H_2O) in CD_3CN (or CH_3CN).

(39) Steemers, F. J.; Verboom, W.; Reinhoudt, D. N.; Vandertol, E. B.; Verhoeven, J. W. *J. Am. Chem. Soc.* **1995**, *117*, 9408.
(40) Latva, M.; Takalo, H.; Mukkala, V. M.; Matachescu, C.; Rodríguez-Ubis, J. C.; Kankare, J. *J. Lumin.* **1997**, *75*, 149.
(41) Petoud, S.; Bünzli, J.-C. G.; Glanzman, T.; Piguet, C.; Xiang, Q.; Thummel, R. P. *J. Lumin.* **1999**, *82*, 69.

ligand excitation. Although the sensitization of the metal ion luminescence remains small, it is noteworthy that the corresponding monometallic Eu(III) cryptate displays a much weaker emission (the quantum yield could not be measured).[14] This has to be traced back to the absence of water and OH groups in the inner coordination sphere of Eu(III) in the dimetallic cryptate. The coordination of the nitrate ion results in an emission spectrum at 10 K that cannot be interpreted in terms of a C_3 symmetry, since the transitions to $^7F_2$ and $^7F_1$ display four and three components, instead of the two and three expected, respectively. This is in apparent contradiction with the NMR experiments, but can be explained because the slower time scale of the NMR experiments results in a time-averaged C_3 symmetry, probably because the nitrate ion is in fast exchange on the NMR time scale at room temperature.

The excitation spectrum of the Tb−Zn cryptate (**7**) recorded in the solid state at 10 K produces a broad band with a maximum at 24 450 cm^{-1}, corresponding to the excitation through the $^1\pi\pi^*$ ligand state. The corresponding emission spectrum displays $^5D_4 \rightarrow {}^7F_J$ transitions at 20 371, 18 354, 17 119, and 15 968 cm^{-1} for $J = 6$, 5, 4, and 3, respectively. It is dominated by the transition to $^7F_5$, as shown by the integrated and corrected relative intensities: 1.00, 2.27, 0.51, and 0.19 for $J = 6$, 5, 4, and 3. This is indicative of sensitization of the Tb(III) ion via a relatively efficient ligand-to-metal energy transfer. However, the energy of the 0-phonon transition lies ca. 2200 cm^{-1} below that of the $^5D_5$ level of the Tb(III) ion. We thus conclude that Tb(III) ($^5D_4$) emission is most efficiently sensitized by the singlet state, as previously observed in Tb(III) complexes with Schiff-base ligands.[42] The lifetime of the $^5D_4$(Tb) state at 10 K is short (ca. 0.8 ms), and the Tb(III) emission is completely quenched at 295 K, which is indicative of a temperature-dependent quenching mechanism such as mixing with ligand vibrational modes or back transfer to ligand excited states. The emission spectrum recorded in frozen acetonitrile solution at 10 K is very similar to the above described in the solid state, but the emission lifetime is slightly longer (ca. 1.0 ms).

Photophysical Properties of the Nd−Zn and Yb−Zn Cryptates. Since L^1 possesses a low-energy triplet state (0-phonon at 18 248 cm^{-1} as measured in the solid state for the Gd−Zn cryptate), it appears that it would be suited for sensitization of Nd(III) and Yb(III) ions. The luminescence spectrum (Figure 9a) of the Yb−Zn cryptate (**12**) recorded in the solid state at 10 K under excitation through the ligand levels at 21 834 cm^{-1} consists of an intense band at 10 243 cm^{-1}, assigned to the $^2F_{5/2} \rightarrow {}^2F_{7/2}$ transition, as well as a group of less intense bands between 10 152 and 9 950 cm^{-1} that we assign to vibronic transitions.[43,14] The spectrum also shows a second less intense band at 10 226 cm^{-1}, which may be assigned to a transition from the lowest excited crystal field component of $^2F_{5/2}$ to an excited crystal field component of $^2F_{7/2}$. However, this second maximum could also arise from the presence of slightly different coordination environments around the Yb(III) ion, as observed for the Yb−Yb analogue.[14] The luminescence spectrum (Figure 9b−d) of the Nd−Zn cryptate displays three bands in the spectral range 11 440−10 850, 9 450−9 120, and 7 550−7 050 cm^{-1} comprised of 5, 6, and 7 main components, respectively. They are assigned to transitions from the $^7F_{3/2}$ level to the $^4I_{9/2}$, $^4I_{11/2}$, and $^4I_{13/2}$ sublevels. The crystal field splitting appears to be consistent with a local distorted C_3 symmetry at the Nd(III) center.

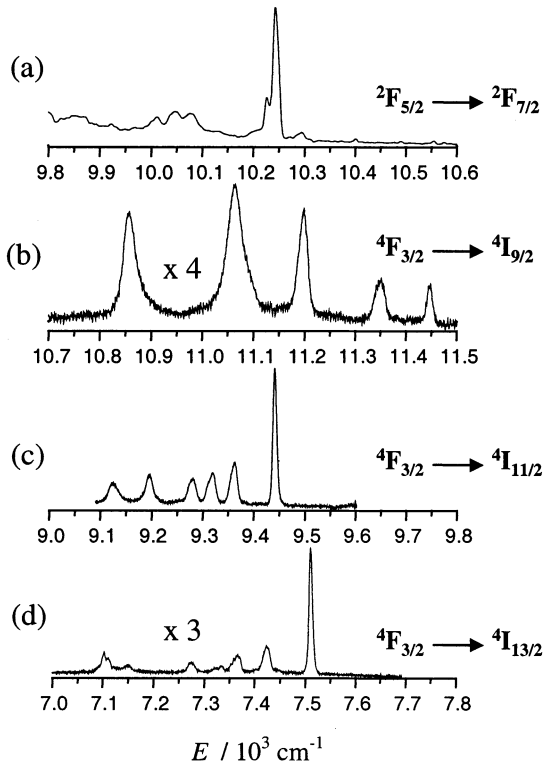

Figure 9. Emission spectra of the (a) Yb−Zn and (b-d) Nd−Zn cryptates at 10 K. Vertical scale: arbitrary units. Nd spectra are normalized with respect to the $^4F_{3/2} \rightarrow {}^4I_{11/2}$ transition.

Conclusions

The X-ray crystal structures of the Pr−Zn (**2**), Yb−Zn (**12**), Lu−Zn (**13**), and Zn−Zn (**15**) cryptates confirm the encapsulation of both metal ions into the cavity at a very short distance. The four cryptates display a helical structure in the solid state. A quantitative analysis of the triple helical structure shows that the Ln(III)−Zn(II) are distorted in the solid state as a consequence of the coordination of a nitrate anion between two chains of the ligand. This is not the case for the Zn(II)−Zn(II) cryptate, which possesses a less distorted helical structure in the solid state. A ^1H NMR study carried out in CD_3CN-D_2O mixtures demonstrates that the helical structure of the Ln(III)−Zn(II) complexes is essentially maintained in solution. However, while in the solid state they adopt conformations $\Lambda(\delta\delta\lambda)_5(\delta'\delta'\delta')_5$ or $\Delta(\lambda\lambda\delta)_5(\lambda'\lambda'\lambda')_5$ in solution the cryptates possess C_3 symmetry $\Lambda(\delta\delta\delta)_5(\delta'\delta'\delta')_5$ or $\Delta(\lambda\lambda\lambda)_5(\lambda'\lambda'\lambda')_5$. The ligand-to-Eu(III)

(42) (a) Howell, R. C.; Spence, K. V. N.; Kahwa, I. A.; White, A. J. P.; Williams, D. J. *J. Chem. Soc., Dalton Trans.* **1996**, 961. (b) Guerriero, P. A.; Vigato, P. A.; Bünzli, J.-C. G.; Moret, E. *J. Chem. Soc., Dalton Trans.* **1990**, 647.
(43) Perkins, W. G.; Crosby, G. A. *J. Chem. Phys.* **1965**, *42*, 407.

energy transfer is fairly efficient at low temperature, but back transfer is implied in the deactivation process, especially at room temperature, because the ligand triplet state lies at very low energy. Although the overall sensitization of the metal ion luminescence remains small, the corresponding monometallic Eu(III) cryptate displays a much weaker emission because the oxygen atoms of the phenolic groups are protonated. The Tb(III) ion is weakly sensitized through the excited singlet state of the ligand. The low energy of the ligand triplet state allows an appreciable conversion of the visible light absorbed into infrared light emitted by Nd(III) and Yb(III), which opens interesting perspectives for the design of new light-converting devices.

Acknowledgment. The authors thank Dr. J. A. Peters (Delft University of Technology, Delft, The Netherlands) for his facilities to record some of the NMR spectra and H. Adams (University of Sheffield, UK) for the X-ray crystal data collection of compounds **2** and **3**. R.R.-C., F.A., C.P.-I., A.deB. and T.R.-B. also thank the Ministerio de Ciencia y Tecnología and FEDER for financial support (BQU2001-0796). J.-C.G.B. and D.I. thank the Swiss National Science Foundation and the Swiss Office for Science and Education (COST D18 action) for financial support and F. Gumy for technical assistance. This research was performed in the framework of the EU COST Action "Lanthanide Chemistry for Diagnosis and Therapy" (D18).

Supporting Information Available: X-ray crystallographic files, in CIF format, for **2**, **12**, **13**, and **15**, and Tables S1 and S2 listing selected angles for these four complexes. This material is available free of charge via the Internet at http://pubs.acs.org.

IC025587S